Dynamic fracture in a discrete model of a brittle elastic solid

Teresa Martín, Pep Español, Miguel A. Rubio, and Ignacio Zúñiga
Departamento de Física Fundamental, Universidad Nacional de Educación a Distancia, C/Senda del Rey s/n, E-28040 Madrid, Spain
(Received 28 July 1999)

Dynamic fracture of brittle materials is studied by means of a molecular dynamics simulation of a two-dimensional (2D) lattice of point particles. By a particular discretization of the continuum equations of elasticity, we derive the Born model in such a way that the model parameters are related to the material properties. Numerical simulations are performed, which show a branching instability, under Mode I loading, occurring at a *critical crack tip speed.* The analysis of the dynamical stress tensor field near the tip shows a qualitative similarity to Yoffe's stress field.

PACS number(s): 62.20.Mk, 46.50.+a, 02.70.Ns, 81.40.Np

I. INTRODUCTION

The understanding of how solid materials break apart when external loads are applied is a crucial safety issue that has attracted the attention of engineers and material scientists for a long time [1]. Quite recently, it has also attracted the attention of physicists, as the complex spatio-temporal dynamics of crack propagation has strong resemblances to other pattern-forming systems and models such as diffusion limited aggregation, dielectric breakdown, or percolation [2].

Different mechanisms of fracture arise depending on the nature of the material. Brittle materials behave as linear elastic solids until a breaking threshold is attained. Ductile materials, on the other hand, display plastic deformations and dislocation motion plays an important role in the dynamics of fracture. Recent well controlled experiments of crack propagation have been conducted in materials such as PMMA or soda lime glass, which have raised considerable interest in brittle materials [3–7].

According to the theory of linear elasticity of brittle materials, the maximum crack speed should be the Rayleigh wave speed V_R [1]. More precisely, the dynamics of a propagating crack along a prescribed straight path can be solved if one assumes that the energy release rate is constant. In this case, the limiting velocity is the Rayleigh wave speed. However, the phenomenology of crack propagation in brittle materials is more complex. Experimental observations in PMMA show that there are no cracks propagating at speeds lower than $\approx 0.18V_R$ or higher than $\approx 0.7V_R$ [3,6]. Moreover, when the crack speed exceeds a critical value around $\approx 0.4V_R$, oscillations on the measured tip velocity appear [3], acoustic emission is important [4,6], and surface roughness appears [3,6]. Several different mechanisms such as dissipation [8], wavy motion [9], or crack branching [5,10] have been proposed to explain this phenomenology.

The theoretical analysis of the dynamic fracture presents difficulties that have allowed for the achievement of only some partial solutions in very simplified situations. The strong nonlinearities of the problem that arise from the coupling between the linear equations of elasticity and the complex boundary conditions due to creation of new surface as the crack propagates make the problem quite intractable, particularly when branching occurs. In this context, numerical simulations appear to be an adequate route to gain some insight into the complexities of the crack evolution. Essentially three main types of numerical simulations have been followed. From a microscopic point of view one can treat the material as composed by atoms, usually in a crystal, and study the evolution of the system when imposed loads are present. This approach was pioneered by Ashurst and Hoover [11] who showed how molecular dynamics simulations could be applied to the study of elasticity problems. Recently, large scale molecular dynamics simulations on two-dimensional (2D) triangular lattices of particles interacting with conservative potentials have provided detailed information about fracture instabilities, crack branching, and dislocation emission [12]. Common features of these microscopic simulations are the anisotropy of the crystal, the presence of complex atomic rearrangements at the crack tip, and the emission of dislocations. These features of plastic crystalline materials can only help us to understand some qualitative features of the experiments conducted on an amorphous polymeric solid like PMMA.

A second approach has been the study of finite lattices, usually triangular ones, with particular laws of force between the points of the lattice and a critical threshold of rupture of bonds [10,13]. These lattices can be understood as models of brittle fracture without the effects of dislocations. The advantage of this approach is that sometimes analytical solutions are available with which we can make comparisons. It is seen that the lattice has strong effects on the dynamics of the crack, giving rise to phenomena like lattice trapping, or the existence of forbidden steady state crack velocities.

Finally, a third approach to the numerical study of dynamic fracture is that of finite elements. Recently, Xu, and Needelman [14] have considered this technique with a continuum model for a rather complex isotropic hyperelastic solid with potential surfaces of decohesion interspersed throughout the material. Crack branching and the dependence of crack velocity with impact velocity are observed features of the simulation.

The picture that emerges from these three approaches is that the spatio temporal dynamics of a fracture model depends on the combination of three main ingredients: the force law, the fracture criterion, and the local geometry of the lattice or the space discretization. However, the influence of fracture criterion and local lattice geometry close to the tip on the dynamics is not well understood. A reasonable first

step in this direction is the investigation of the fracture dynamics in a discrete model that would represent an ideally elastic brittle solid at large length scales. The behavior of such a model should mimic reasonably well the behavior of a brittle elastic solid, which is linearly elastic and isotropic at large length scales, and discrete at small length scales.

In this work we construct a discrete lattice model from the continuum equations of elasticity that respects the properties of isotropy and linear elasticity at large length scales. Our discretization procedure leads to a finite difference scheme in a triangular lattice that appears in a tensorial form, thus allowing for an interpretation of the nodes of the mesh as actual particles (rather as mesoscopic portions of material), which interact with prescribed laws of force. The resulting force law coincides with the Born model [15], which has been used extensively in studies of quasielastic and dynamic fracture [16]. Interestingly, our discretization scheme provides for precise formulas relating the elastic constants in the Born model with the transverse and longitudinal wave sounds speeds of the material. Moreover, the general discretization scheme can also be implemented for different lattice geometries, as well as next nearest neighbor interaction, or different constitutive equations.

The discrete equations of motion have been simulated by means of a conventional molecular dynamics algorithm [17]. The model allows for the study of *dynamic* fracture, in which the crack speed is close to the Rayleigh wave speed. This is at variance with studies of quasielastic fracture in which after bond breaking the system is allowed to relax before a new bond breaks [16]. In this sense, the model presented in this paper can be understood as an extension of the previous model for quasielastic fracture in Ref. [16] to the dynamical regimes in which the crack speed is comparable to the sound speeds. In the present study we have implemented a deterministic fracture criterion based on a given threshold deformation, the usual brittle one in which a single bond breaks when a critical deformation is reached. Our aim here is to make a comparison with analytical results of dynamical fracture in linear elasticity as a first check of the model. Of course, the implementation of a probabilistic fracture criterium as in Refs. [16] would take into account interesting effects of disorder of finite temperature.

In this paper, we show that the expected linear elastic behavior is obtained for sound waves with wavelengths larger than seven lattice spacings. We present also numerical results on crack propagation under Mode I loading. The loading level is controlled by cutting an initial notch with an adjustable length. As the fracture criterion, we have taken the usual brittle one in which a single bond breaks when a critical deformation is reached. In the simulations the crack moves in a straight line and accelerates until the tip reaches a critical velocity V_c. The value of V_c appears to be independent of the loading level. When the crack tip reaches this critical velocity, the crack branches into two macroscopic running cracks.

The existence of a critical crack tip velocity for macroscopic branching suggests that perhaps mechanisms such as those proposed after Yoffe's stress field solution [18,1,19] might be in action. In order to assess whether one of those mechanisms is operating in the discrete lattice, we have studied the azimuthal angle dependence of the stress field close to the tip. Although qualitative agreement is observed, the strong effects due to the local lattice geometry near the tip do not allow us to draw strong conclusions about the physical mechanism involved.

The paper is organized as follows. In Sec. II, we present the model equations and discuss the implementation of the fracture criterion. Section III is devoted to the simulation results related to wave and crack propagation. In Sec. IV we show the results concerning the spatial structure of the stress field close to the tip making a comparison with the analytical curves obtained in the Yoffe analysis. The discussion and conclusions are presented in Sec. V. Details of the discretization scheme are given in the Appendix.

II. DISCRETE MODEL FROM ELASTICITY EQUATIONS

The linear equations of elasticity that govern the displacement field $\mathbf{u}(\mathbf{r},t)$ in an homogeneous material subject to small deformations are [1]

$$\ddot{\mathbf{u}}(\mathbf{r},t)=c_\perp^2\nabla^2\mathbf{u}(\mathbf{r},t)+(c_\parallel^2-c_\perp^2)\nabla(\nabla\cdot\mathbf{u})(\mathbf{r},t), \tag{1}$$

where the transverse $c_\perp$ and longitudinal $c_\parallel$ sound speeds are material properties related to Young's modulus E and Poisson's coefficient ν through

$$c_\perp=\left(\frac{E}{2\rho(1+\nu)}\right)^{1/2},$$

$$c_\parallel=\left(\frac{E(1-\nu)}{\rho(1+\nu)(1-2\nu)}\right)^{1/2}. \tag{2}$$

Here, ρ is the mass density of the material. A third speed can be defined in a material, that of the surface waves propagating on the free boundaries of the material. For the purposes of this study, the surface Rayleigh wave speed may be approximated by the expression [20]

$$V_R\approx c_\perp(0.874+0.162\nu). \tag{3}$$

We have discretized the elasticity equations (1) following a general procedure that allows us to discretize partial differential equations in an arbitrary lattice (including random ones). The procedure is constructed from the point of view of an optimization problem; full details are given in the Appendix. In this paper, we consider only triangular lattices for which the expressions simplify considerably. As shown in the Appendix, the discrete equations corresponding to (1) are

$$\ddot{\mathbf{u}}_i(t)=\left[\frac{c_\perp^2-c_\parallel^2/3}{a^2}\right]\sum_{j=1}^{6}(\mathbf{u}_j-\mathbf{u}_i)+\frac{4(c_\parallel^2-c_\perp^2)}{3a^2}\sum_{j=1}^{6}(\mathbf{u}_j-\mathbf{u}_i)\cdot\hat{\mathbf{r}}_{ji}^0\hat{\mathbf{r}}_{ji}^0, \tag{4}$$

where a is the lattice spacing and $\hat{\mathbf{r}}_{ji}^0$ is the underformed lattice vector joining particles j and i. These equations are second order ordinary differential equations that can be interpreted as the equations of motion for a set of particles of unit mass in a lattice, interacting with its nearest neighbors with a linear law of force. The force has two components, a

first one that represents a linear spring connecting the particles and a second one that is directed to the equilibrium positions of the particles (it is a sort of biased linear spring). The elastic constants of these two types of springs are given in terms of the shear and sound speeds.

It is worth noting that the above discrete model coincides with the Born model that has been used in several studies of quasistatic and dynamic crack propagation [16]. The Born model is characterized by the following potential energy

$$V=\frac{1}{2}(\alpha-\beta)\sum_{ij}\ [(\mathbf{u}_i-\mathbf{u}_j)\cdot\hat{\mathbf{r}}_{ji}^0]^2+\frac{1}{2}\beta\sum_{ij}\ [\mathbf{u}_i-\mathbf{u}_j]^2, \tag{5}$$

where α,β are model constants that are tuned at will. The force on particle i derived from this potential energy is

$$\mathbf{F}_i=\frac{\partial V}{\partial \mathbf{u}_i}=(\alpha-\beta)\sum_j\ (\mathbf{u}_j-\mathbf{u}_i)\cdot\hat{\mathbf{r}}_{ji}^0\hat{\mathbf{r}}_{ji}^0+\beta\sum_{ij}\ (\mathbf{u}_j-\mathbf{u}_i), \tag{6}$$

which coincides with the force in Eq. (4). We have, therefore, provided a physical meaning to the model constants α,β in terms of the sound speeds $c_\perp, c_\parallel$.

The physics encoded in the linear elasticity equation (1) is quite simple: any perturbation of the displacement field can be decomposed in terms of sound and shear waves, each propagating independently at its own speed. Despite this simplicity, the presence of nontrivial boundary conditions make elasticity problems difficult to solve. The difficulty is even larger for fracture problems because the boundary conditions are coupled with the dynamics of the fields. In order to specify this coupling it is necessary to formulate a fracture criterion that states when one fracture surface is created. The fracture criterion is, from a conceptual point of view, an additional physical ingredient as important as the constitutive equation of the material.

Which is the best fracture criterion for ''brittleness''? This is not an easy question to answer from a continuum point of view. Different criteria lead to different dynamical behavior. A usually chosen criteria is that stating that a sharp crack tip moves when the stress intensity factor overcomes some material dependent threshold. However, this is an incomplete prescription because it does not specify the *direction* of the propagating crack. Several further specifications must be made, for example, that the crack will move in the direction of the maximum circumferential stress [18], or in the direction of the eigenvector of smaller eigenvalue of the stress tensor [21]. See Ref. [19] for still another formulation for a fracture criterion.

On a lattice model it seems natural to use as fracture criterion the simplest one based on the idea of brittle springs that respond elastically until they break at a critical deformation. The physical picture in a real material is that two points representing portions of material that interact elastically will stop interacting if they separate more than the range r_c of the cohesive force. This is a simplistic picture of al the complex physics of real materials but it provides a precise fracture criterion. Note that in a lattice it is not necessary to specify the direction that the crack will follow. The mathematical formation of this fracture criterion is as follows. Let us take a pair of nodes i,j of the lattice and consider the displacement field $\mathbf{u}_i$ and $\mathbf{u}_j$ in each node. The length of the bond connection i and j will be

$$\begin{aligned} dl^2&=(\mathbf{u}_j-\mathbf{u}_i+\mathbf{r}_{ji}^0)^2\\ &\approx[a+2(\mathbf{u}_j-\mathbf{u}_i)\cdot\mathbf{r}_{ji}^0+(\mathbf{u}_j-\mathbf{u}_i)\cdot(\mathbf{u}_j-\mathbf{u}_i)]. \end{aligned} \tag{7}$$

If this length exceeds r_c for some of the six neighbors j of i, the bond i,j will break. This is $dl^2>r_c^2$. For small deformations of the quadratic terms ar negligible and

$$dl\approx a[1+(\mathbf{u}_j-\mathbf{u}_i)\cdot\mathbf{r}_{ji}^0]>r_c. \tag{8}$$

This can be written as

$$(\mathbf{u}_j-\mathbf{u}_i)\cdot\mathbf{r}_{ji}^0>\gamma_c, \tag{9}$$

with the critical strain $\gamma_c=(r_c-a)/a$.

Equations (4) have been simulated with a conventional molecular dynamics code using Verlet's algorithm (i.e., a centered difference in time) [17]. This is an explicit method in the language of finite differences simulations. If a particular bond fulfills the condition (9) then we remove the particle j from the Verlet's neighbor list of particle i [17]. In this way particle i and j are not considered neighbors any more and no longer interact. We preclude, thus, the possibility of surface recombination. Some trial runs were also performed allowing for surface recombination but no effects on the dynamics of the model were observed.

For latter reference, we present now the discrete expressions for the stress and strain tensors. The strain tensor is defined in the continuum theory as $\gamma=\frac{1}{2}[\nabla\mathbf{u}+\nabla\mathbf{u}^T]$. By using the discretization of first derivatives presented in the Appendix, we obtain the following expression for the strain tensor defined at each node of the mesh,

$$\gamma_i=\frac{1}{6a}\sum_j\ (\mathbf{u}_i-\mathbf{u}_j)\hat{\mathbf{r}}_{ji}^0+\hat{\mathbf{r}}_{ji}^0(\mathbf{u}_i-\mathbf{u}_j). \tag{10}$$

The stress tensor $\boldsymbol{\sigma}_i$ at the node i is given in terms of the strain tensor according to [20]

$$\sigma_i=\frac{E}{1+\nu}\left(\gamma_i+\frac{\nu}{1-2\nu}\,\mathrm{tr}\,\gamma_i\mathbf{1}\right), \tag{11}$$

and reciprocally

$$\gamma_i=\frac{1}{E}[(1+\nu)\boldsymbol{\sigma}_i-\nu\,\mathrm{tr}\,\boldsymbol{\sigma}_i\mathbf{1}]. \tag{12}$$

One caveat is in order here: the discretization procedure has some merits, for instance, the applicability to problems with different constitutive equations, different lattice geometries, and arbitrary number of neighbor interactions. However, it does not guarantee that the particular simulation scheme obtained in a given situation is stable. In fact, the simplest simulation scheme that we present here is unstable for $\nu>0.25$; this particular value of the Poisson coefficient is the one at which the coefficient of the linear spring force in Eq. (4) changes sign. This problem is eliminated by recalculating the force law considering also next nearest neighbors interaction [22].

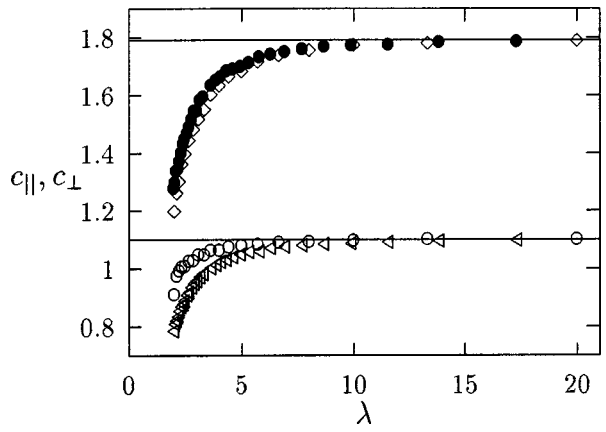

FIG. 1. Dispersion relations: The speed of propagation of a wave (in units of the Rayleigh wave speed) as a function of the wavelength λ (in units of the lattice spacing a). $c_{\|}$ for longitudinal waves with the wave number **k** parallel (●) and perpendicular (◇) to a lattice direction and $c_{\perp}$ for transverse waves with the wave number **k** parallel (△) and perpendicular (○) to a lattice direction. Solid lines are the continuum values $c_{\perp}=1.10$ and $c_{\|}=1.79$.

III. SIMULATION RESULTS: WAVE AND CRACK PROPAGATION

A. Dispersion relations and isotropy

We have selected a Poisson number of $\nu=0.2$. We take as units of space the lattice spacing and as units of velocity the Rayleigh wave speed ($V_R=1$). This sets the unit of time. The theoretical shear and longitudinal sound speeds are from Eqs. (2), (3), $c_{\perp}=1.10$, and $c_{\|}=1.79$. Even though the original continuum model of linear elasticity (1) is dispersionless, the discretization always produces dispersion at small length scales. In order to quantify this dispersion, we have induced shear and longitudinal waves in a 2D lattice with periodic boundary conditions in both directions and have checked that the speed of the waves depends on the wave number. The results are presented in Fig. 1. Four types of waves have been induced in the plate: longitudinal waves with the wave number **k** parallel (bullets) and perpendicular (diamonds) to a lattice direction and transverse waves with the wave number **k** parallel (triangles) and perpendicular (open circles) to a lattice direction. Nevertheless, for $\lambda>7$ both longitudinal and transverse waves with **k** parallel or perpendicular to lattice directions coincide perfectly with the corresponding continuum values.

We observe that for wavelengths smaller that $\lambda\sim 7$ the longitudinal and transversal speeds of sound are smaller than the corresponding continuum values. In addition, we observe that for these small wavelengths the lattice is not isotropic. A transverse wave moves faster in the directions of the lattice vectors than in the directions perpendicular to the lattice vectors. This anisotropy effect is not so pronounced for longitudinal waves.

B. Crack propagation

We have studied Mode I fracture of finite 2D rectangular plates of dimensions $L_x\times L_y$ that contain an initial sharp notch of length L_n. The notch is located in the middle of the plate and is made by cutting the transversal bonds on the central column starting from the upper boundary (see Fig. 2).

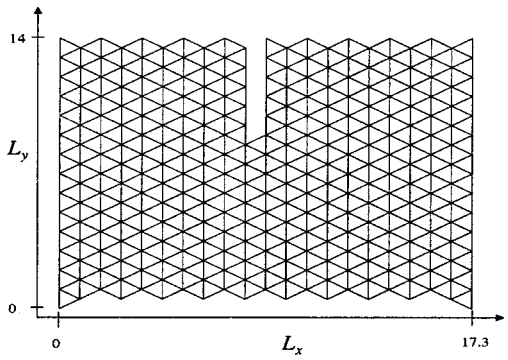

FIG. 2. Triangular lattice with a lattice direction along the vertical y direction. In this small lattice considered for illustration, a notch of $L_n=8$ is made by cutting transversal bonds at the middle of the plate. The lattice is stressed by producing a displacement ΔL_x of the right vertical boundary. L_x and L_y are in units of the lattice spacing.

Typical plates of 80.000 particles are studied. The plate is subject to a Mode I deformation by displacing the particles of the right wall a fixed distance ΔL_x in the x direction. The plate is left to equilibrate until the stationary stress field corresponding to the given geometry is reached. A damping force is applied to each particle during this equilibration time in order to speed up the equilibration and get rid of the traveling waves due to the application of the deformation. The equilibration time is several times that required by sound waves to travel the sample. In this way, we are starting the simulation with all particles at rest and, effectively, reproducing the experimental conditions of quasielastic loading before fracture initiation.

In principle, two different types of numerical simulations can be performed, at a given critical strain γ_c or at a given nominal deformation ϵ, where $\epsilon=\Delta L_x/L_x$. In the first case (critical strain γ_c fixed), we have to compute the nominal deformation ϵ_c at which fracture occurs. This can be achieved easily by means of a previous run in which the equilibrium maximum strain $\overline{\gamma}$ in the notched plate is obtained for a given deformation $\overline{\epsilon}$. Because $\overline{\gamma}=\alpha\overline{\epsilon}$, where α is a coefficient of proportionality, we have $\epsilon_c=\overline{\epsilon}\gamma_c/\overline{\gamma}$ [23]. We note that for critical strain fixed, by increasing the number of nodes we are increasing the *size* of plates of the same material. The reason is that by fixing the critical strain γ_c one is fixing a length scale r_c.

The second kind of experiment that can be performed is at a given nominal deformation ϵ. In this case, we have to adjust the critical strain by computing the deformation of the most stretched bond and the next most stretched bond. By selecting the average value between these two deformations we make sure that at the beginning of the dynamical run only the most stretched bond will break, thus triggering the propagation of the crack. The simulations that will be presented are performed with this second kind of experiment, with a given nominal deformation of $\epsilon=0.01$. Note that at fixed nominal deformation, by increasing the number of nodes in the plate we are increasing the *resolution* of the plate. The idea is that if plates of equal geometry but different number of nodes all break at the same nominal deformation they will correspond to different representations of the same plate of the same material.

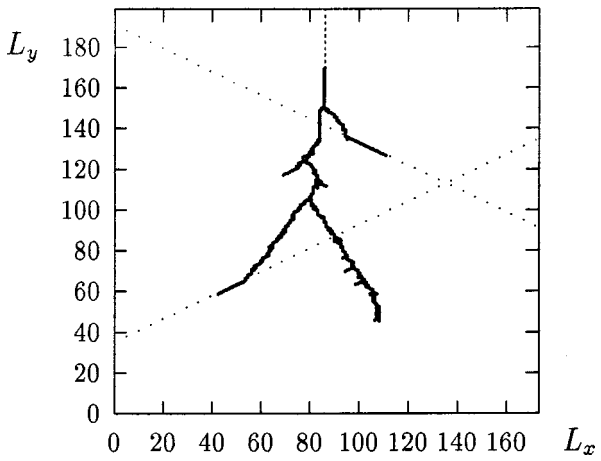

FIG. 3. Record of all broken bonds in a plate. Both axes are in units of the lattice spacing a. Dotted straight lines are two lattice directions to guide the eye (the third lattice direction is vertical). Vertical slashed line is the initial notch with $l_n=60$. L_x and L_y are in units of the lattice spacing.

We have conducted a series of simulations in which the effect of the notch length on the dynamics of crack propagation is studied systematically. The notch length determines the level of stress of the landscape on which the crack propagates and it is usually the way in which this effect is investigated experimentally (also the shape of the notch is relevant experimentally). Plates with long notches require smaller levels of deformation to break. In Ref. [24] we studied the effect of notch length on crack fracture of an anisotropic model and a full discussion of the dependence of the maximum stress in the plate as a function of notch length was presented.

In Fig. 3 we show a plate in which the lattice is oriented with a lattice direction along the vertical. In this case $\nu=0.25$ and the initial notch has a length of $l_n=60$. The plate is let to equilibrate without breaking until a static state is reached. At that point the breaking strain threshold γ_c is adjusted just below the deformation of the most stretched bond. A crack is initiated and it propagates in a straight line along the vertical lattice direction. The crack branches at a given time in two cracks and the subsequent motion is irregular with several attempted branching. We plot in Fig. 3 a record of all the broken bonds of the plate until a given time. It should be noted that the main branches do not follow the lattice directions in the major part of their development.

In order to study the velocity of the crack tip, we define the position of the tip as the middlepoint of the most advanced breaking bond. The tip velocity is calculated by dividing the y coordinate difference by the time interval in between the last two most advanced broken bonds. This definition is the closest to the experimental measurement of the crack tip velocity [3,6], which basically measures the resistance of the metallic strip in between the most advanced crack tip and the free border of the breaking plate. The time history of the velocity for the crack tip in Fig. 3 is shown in Fig. 4. The crack starts moving at a finite velocity (≈ 0.6), which is different from zero due to the essential discrete way of computing the velocity. At short times ($t<10$) the crack propagates in a straight line and small oscillations of the tip velocity occur. These velocity oscillations disappear at t

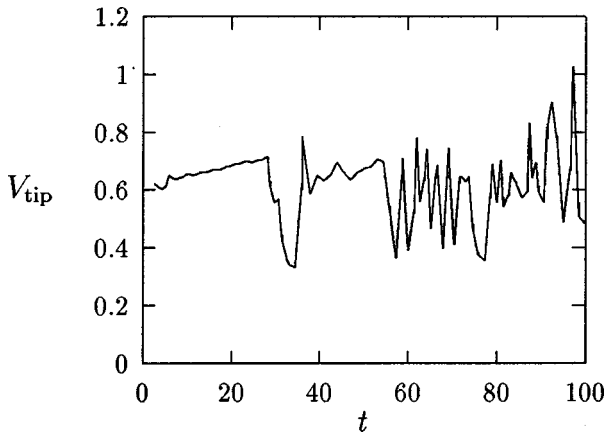

FIG. 4. Crack tip velocity (in units of the Rayleigh wave speed) as a function of time (in units of a/v_R). The strong oscillations are due to the branching.

~ 10; from then on the crack propagation is still straight and the tip velocity grows in a rather linear way until $t\sim 25$ when branching starts. Before branching occurs, the acceleration of the crack tip decreases as the notch length decreases, i.e., as the stress level is higher.

Once branching has started very strong tip velocity fluctuations are observed. These wild fluctuations are caused by the branching process in which the most advanced broken bond can belong to different branches at different times. For instance, tip velocities higher than unity appearing in Fig. 4 correspond to one branch surpassing another, with a small time interval in between the breaking of the most advanced bonds of both branches.

The main observation here is that branching occurs at the same value of tip velocity irrespective of notch length, i.e., there is a well defined critical tip speed for branching to happen, within the simulation error. This is shown in Fig. 5 where the velocity of the crack tip at the branching point is represented as a function of the notch length. For all cases branching occurs when the crack tip reaches the critical velocity $V_c=0.71\pm 0.01$.

Recently, it has been proposed that in experiments of Mode I fracture in PMMA [7], the branching instability is

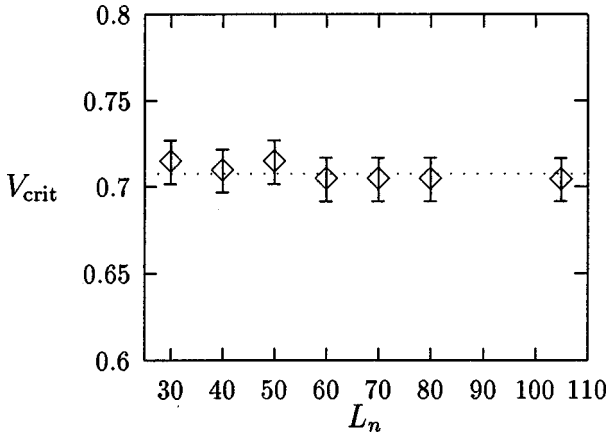

FIG. 5. The velocity of the crack (in units of the Rayleigh wave speed) at the moment of branching for each notch length (in units of the lattice spacing a). The dotted line is the average value $V_c=0.71$.

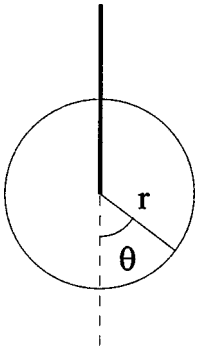

FIG. 6. Polar coordinates with respect to the crack tip. Solid vertical line is the crack.

triggered by the reflection against the boundaries of sound waves generated during the cracking process. This is not so in the present simulations, because here the crack tip speed is higher than in the referred experiments and therefore branching occurs always at a time smaller than that required by the longitudinal waves to travel back and forth to the nearest boundary.

IV. SIMULATION RESULTS: STRUCTURE OF THE STRESS FIELD

The existence of a critical branching velocity and its particular value in a model that represents well a linear elastic solid at large length scales calls for a comparison with the stress field derived by Yoffe [18]. In any case the comparison should be taken with some care because Yoffe's solution is valid asymptotically close to the tip and, due to the discrete nature of the model, the isotropy and linear elasticity of the continuum equations are not preserved at small length scales. We will first succinctly review the main results for the asymptotic fields near a moving crack tip in Mode I loading.

A. Yoffe's stress field

The results given by Yoffe correspond to a crack moving at constant velocity through an infinite plate. Even though the original derivation of Yoffe was made considering cracks moving at constant speed, it is possible to prove that for a linear crack at arbitrary speed, the stress field asymptotically near the tip of the crack has the following form (using polar coordinates as in Fig. 6) [1]:

$$\sigma(r,\theta,v,t)=\frac{K_1(t)}{\sqrt{2\pi r}}\Sigma^I(\theta,v). \tag{13}$$

Here, the dimensionless angular functions Σ_{ij} in Cartesian coordinates, with the x axis in the direction of propagation of the crack, are given by [1]

$$\Sigma^I_{xx}=\frac{1}{D}\left\{(1+\alpha_s^2)(1+2\alpha_d^2-\alpha_s^2)\frac{\cos\frac{1}{2}\theta_d}{\sqrt{\gamma_d}}-4\alpha_s\alpha_d\frac{\cos\frac{1}{2}\theta_s}{\sqrt{\gamma_s}}\right\},$$

$$\Sigma^I_{xy}=\frac{2\alpha_d(1+\alpha_s^2)}{D}\left(\frac{\sin\frac{1}{2}\theta_d}{\sqrt{\gamma_d}}-\frac{\sin\frac{1}{2}\theta_s}{\sqrt{\gamma_s}}\right), \tag{14}$$

$$\Sigma^I_{yy}=-\frac{1}{D}\left\{(1+\alpha_s^2)^2\frac{\cos\frac{1}{2}\theta_d}{\sqrt{\gamma_d}}-4\alpha_s\alpha_d\frac{\cos\frac{1}{2}\theta_s}{\sqrt{\gamma_s}}\right\},$$

with

$$\alpha_d=\sqrt{1-(v/c_d)^2},$$

$$\alpha_s=\sqrt{1-(v/c_s)^2},$$

$$\gamma_d=\sqrt{1-(v\sin\theta/c_d)^2},$$

$$\gamma_s=\sqrt{1-(v/\sin\theta/c_s)^2},$$

$$\tan\theta_d=\alpha_d\tan\theta,$$

$$\tan\theta_s=\alpha_s\tan\theta,$$

$$D=4\alpha_s\alpha_d-(1+\alpha_s^2)^2. \tag{15}$$

The Rayleigh wave speed is the nonzero real root of $D(v)$.

The stress in polar coordinates is given by

$$\sigma_{rr}=\sigma_{xx}\cos^2\theta+\sigma_{xy}\sin 2\theta+\sigma_{yy}\sin^2\theta,$$

$$\sigma_{r\theta}=(\sigma_{yy}-\sigma_{xx})\sin 2\theta+\sigma_{xy}\cos 2\theta,$$

$$\sigma_{\theta\theta}=\sigma_{xx}\sin^2\theta-\sigma_{xy}\sin 2\theta+\sigma_{yy}\cos^2\theta. \tag{16}$$

These expressions allow us also to compute the corresponding strain fields $\gamma(r,\theta,v,t)$ and $\Gamma^I(\theta,v)$ through Eq. (12). The circumferential tensile stress $\sigma_{\theta\theta}$ (also called hoop stress) has an interesting behavior as a function of the velocity of the crack. For crack speeds less than about 60 maximum value of $\sigma_{\theta\theta}$ appears at $\theta=0$. As speed increases, the hoop stress develops a maximum in a direction inclined at an angle from the direction of crack growth different from zero. Yoffe suggested that this inertia induced modification of the local singular stress field could make the crack bifurcate into several branched cracks. In Fig. 7 we plot the angles at which $\sigma_{\theta\theta}$ and $\gamma_{\theta\theta}$ have their maxima as a function of the velocity of the crack. The angles at which the maxima appear increase monotonically from zero to a value beyond 60° as the velocity increases provided that some critical value of the velocity are exceeded. These critical values for the hoop strain and stress are 0.659 and 0.688, respectively. Moreover, above the critical values, $\theta_{\max}$ behaves as the square root of the relative difference between the tip speed and the corresponding critical velocity.

B. Simulation stress field: static crack

We will first consider the structure of the static stress field prior to crack evolution in a plate with a long initial notch. Keeping in mind that Yoffe's expressions are asymptotic fields valid close to the crack tip we need to know the stress tensor obtained from the simulations on a circle of a small radius centered at the crack tip. Information on the radius of the circle can be gained by looking for the expected $r^{-1/2}$ behavior for values of θ close to zero. In Fig. 8 we show the dependence of $\sigma_{\theta\theta}$ on r calculated at the lattice nodes located in the two vertical lines at both sides ahead of the crack tip.

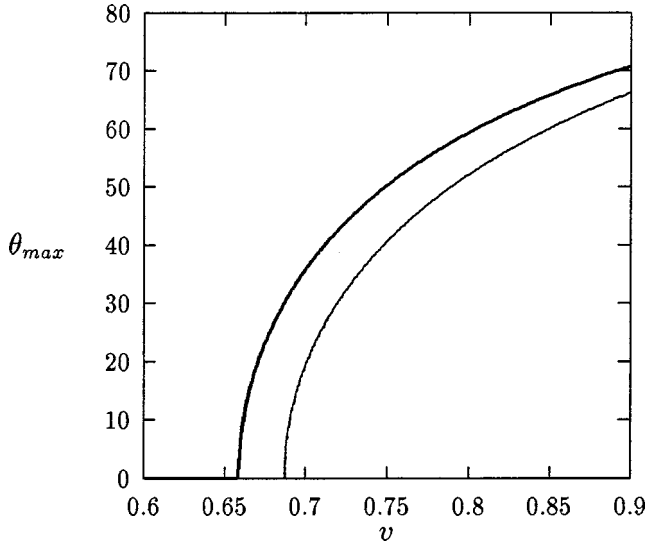

FIG. 7. Angle (in degrees) at which $\Sigma_{\theta\theta}$ (thin line) and $\Gamma_{\theta\theta}$ (thick line) have their maxima, as a function of the crack velocity (in units of the Rayleigh wave speed). The Poisson coefficient is $\nu=0.25$.

It can be seen that within a distance to the tip of three lattice spacings the stresses obtained in the simulation agree reasonably well with the expected $r^{-1/2}$ dependence. Beyond this distance to the crack tip, the stresses decay somewhat slower that $r^{-1/2}$. Therefore, it seems reasonable to take a circle of radius three lattice spacings in order to study the structure of the stress field close to the tip. Unfortunately, because of the discrete nature of the system, the number of lattice nodes within that circle of radius $R=3$ is small.

In the following we will represent the azimuthal dependence of the stress field obtained in the simulations at those lattice nodes that are located within a circle of $R=3$, and the corresponding values at the same points obtained through the

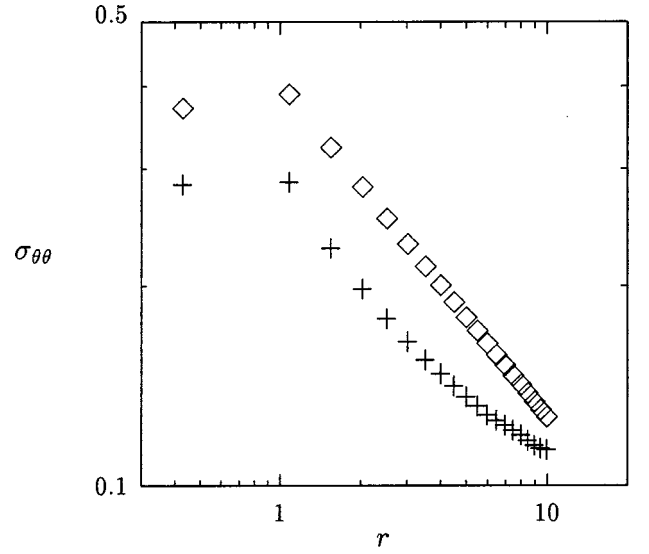

FIG. 8. Dependence of $\sigma_{\theta\theta}$ on r for the lattice nodes in the columns at right and left from the straight propagating crack. Diamonds correspond to Yoffe's stress field and crosses to simulation results. The simulation results here have been shifted by a multiplicative factor.

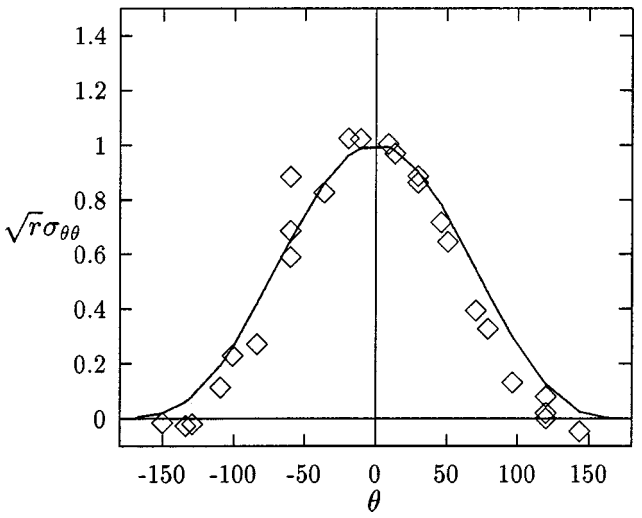

FIG. 9. Plot of $\sqrt{r}\sigma_{\theta\theta}$ (normalized with its value at the angle closest to $\theta=0$) against the angle θ (in degrees) for a static crack. Solid line corresponds to the theoretical expression and diamonds are the simulation results.

expressions (14) and (16). The values of $\sigma_{\theta\theta}$ obtained from the simulations have been multiplied by $\sqrt{r}$, and divided by the value at $\theta=0$, in order to compare with the theoretical expressions for $\Sigma_{\theta\theta}$ computed at the same lattice nodes. All the following data correspond to a plate with $L_x=173.2$, $L_y=399.5$, and notch length $L_n=195$, which is allowed to relax without breaking until a static configuration is reached. This notch length ensures that the crack tip is not affected by the upper and lower boundaries. The stress field around the tip will be, therefore, similar to the infinite strip case [25]. In Fig. 9 we plot $\sqrt{r}\sigma_{\theta\theta}$ against the angle θ for this static configuration. Diamonds correspond to the simulation points and solid line is the Yoffe's field for $v=0$.

A nice overall agreement between the simulation and theoretical results is observed. However, there are some slight differences that can be attributed to several causes. First, one observes that the simulation results are distributed in a narrower curve around $\theta=0$ than the theoretical ones. This might be due to the finite dimensions of the plate; from the map of isolines of stress (normalized with the strip width) in [25] one concludes that the angular distribution of stresses is more localized around $\theta=0$ for a strip of finite width than for a ''strip'' of infinite width. Second, the nonsmooth appearance of the points (see, for instance, at $\theta=-60°$) is a systematic lattice effect that will be discussed below. Finally, the crack tip location is subject to certain ambiguity. The most natural way to define the location of the crack tip appears to be the middle point of the breaking bond at the time the bond breaks; but positions slightly more advanced or retarded might be arguable too. However, we have checked that considering these more advanced or retarded positions for the crack tip merely changes the azimuthal dependence shown in Fig. 9 in a geometrical way, i.e., the azimuthal angles corresponding to the different lattice nodes change by changing the position of the origin of the polar coordinate system located at the crack tip.

C. Simulation stress field: moving crack

We have analyzed the stress field of moving cracks at times long enough that the initial oscillations have decayed

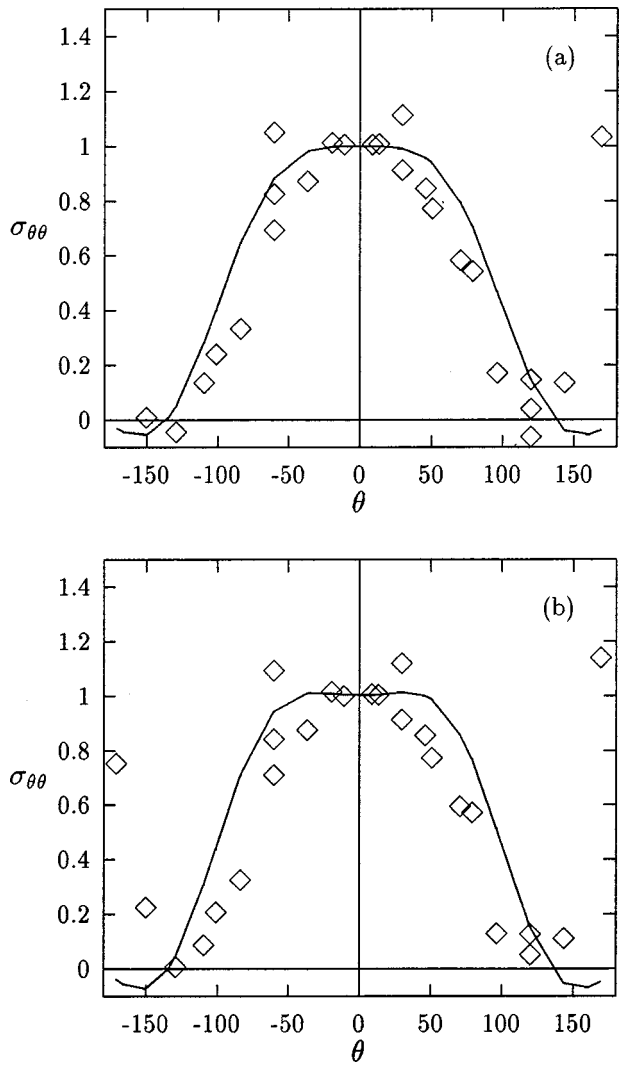

FIG. 10. Plot of the hoop stress $\sigma_{\theta\theta}$ (normalized with the value closest to $\theta=0$) against angle θ (in degrees) from the direction of crack growth at times (a) $t=19.17$ and (b) $t=35.22$. solid line is the asymptotic field and diamonds represent the simulation results.

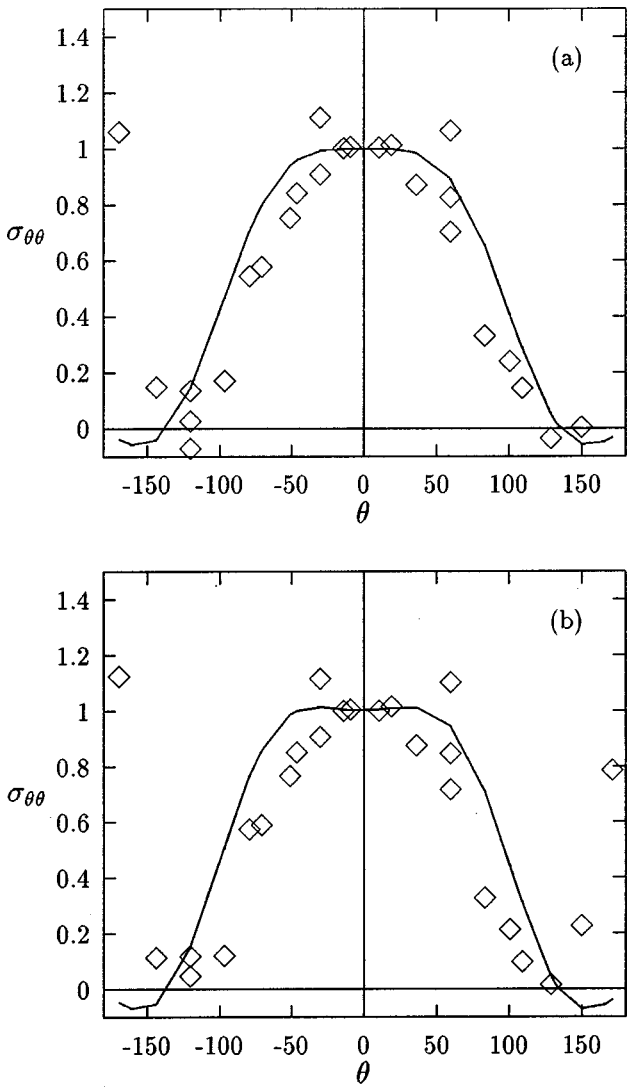

FIG. 11. Plot of the hoop stress $\sigma_{\theta\theta}$ (normalized with the value closest to $\theta=0$) against angle θ (in degrees) from the direction of crack growth at times (a) $t=19.93$ and (b) $t=35.93$. Solid line is the asymptotic field and diamonds represent the simulation results.

and the crack is moving with low acceleration, up to times immediately before branching occurs. In the following the stress fields are represented at times coinciding with the breaking of a bond.

First of all, let us point out that the effects of the lattice asymmetry close to the tip are stronger in the case of a moving crack. In Figs. 10 and 11 the hoop stress is shown at different times (and, therefore, at different crack tip velocities) before branching, plotted against angle θ, as well as the corresponding theoretical values for the same tip velocities. For this particular plate and notch length, the time at which the crack branches is 35.93.

Figures 10(a) and 10(b) correspond to times $t=19.17$ and $t=35.22$, respectively, at both of which the corresponding breaking bond has an inclination of $\theta=60°$; the respective tip speeds are 0.66 and 0.70. Conversely, Figs. 11(a) and 11(b) correspond to times $t=19.93$ and $t=35.93$, respectively, at both of which the corresponding breaking bond has an inclination of $\theta=-60°$; the respective tip speeds are 0.67 and 0.71.

A detailed comparison between Figs. 10 and 11 shows that when the breaking bonds have the same orientation, the hoop stresses have very similar structures at different times. More strikingly, it can be observed that Fig. 10(a) and Fig. 11(a) are specular images of each other with respect to $\theta=0$ [the same applies to Figs. 10(b) and 11(b)]. This comparison clearly shows that the lattice has a strong influence on the stress field near the crack tip and that this influence is systematic.

Figures 10(b) and 11(b), which correspond to tip speed values higher than the critical values of Fig. 7, show that the theoretical hoop stress has already a maximum at $\theta\neq0$. However, in the simulation results, the strong lattice influence forbids an interpretation of the branching as caused by the existence of maxima in the hoop stress at $\theta\neq0$. Actually, it can be seen that there are two nodes (the nearest to the crack tip) at angles 60° and $-30°$ at which the value of $\sigma_{\theta\theta}$ is larger than the value at angles close to 0°. The appearance of these maxima at nodes close to the tip might be due to the method used for computing the stress field through Eqs. (10),

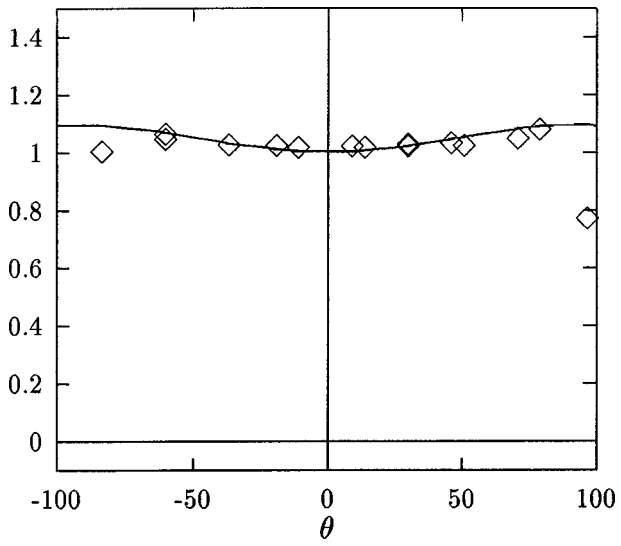

FIG. 12. Theoretical (solid line) and simulation results (diamonds) for the ratio between the hoop stress for times $t=19.17$ and $t=35.22$ corresponding to Figs. 10(a) and 10(b) (angle θ in degrees).

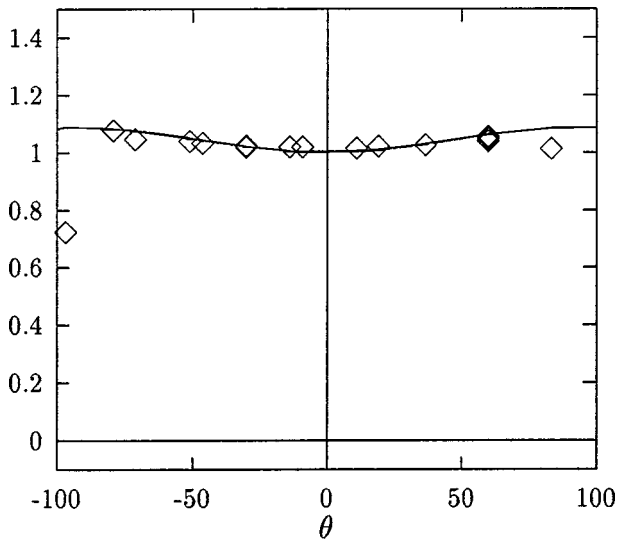

FIG. 13. Theoretical (solid line) and simulation results (diamonds) for the ratio between the hoop stress for times $t=19.93$ and $t=35.93$ corresponding to Figs. 11(a) and 11(b) (angle θ in degrees).

(11), which is, essentially, the finite difference calculation. Very close to the crack tip, where there are very strong variations of the displacement field, this finite difference calculation might give a poor approximation to the stress field.

A surprising fact is that the effects of the lattice structure appear to be mainly multiplicative, and so they may be strongly reduced by dividing the stress fields at different times provided that the orientation of the breaking bond is the same. In Fig. 12 we show the ratio between the stress fields in Figs. 10(a) and 10(b). The solid line is the quotient between the analytical results, whereas the diamonds correspond to the ratio between the simulation results; angles outside the range $(-100,100)$ have not been represented; because of the stress values in the denominator being smaller, large values of the quotient are obtained. We observe that this procedure practically eliminates the systematic lattice effects and also shows a striking coincidence between theory and simulations. The same procedure has been carried out in Fig. 13 where the quotient between data in Figs. 11(a) and 11(b) is presented.

These results suggest that in spite of the strong lattice effects that occur near the crack tip, the azimuthal dependence of the hoop stress that is observed in the simulations captures many of the features of Yoffe's stress field.

V. DISCUSSION AND CONCLUSIONS

Our aim in this paper has been to define from a numerical point of view a model that represents brittle linear elasticity. The approach we follow is a discretization of the continuum equations in a way that the nodes of the grid can be interpreted as actual ''particles'' or portions of material. The resulting algorithm can be interpreted then as a molecular dynamics algorithm instead of a finite difference algorithm in much the same spirit as smoothed particle applied mechanics [26]. Actually, the model obtained is essentially the Born model, with the bonus that the constants appearing in the model are explicitly related to the material properties characterized by the two speeds of sound of the elastic material.

We have studied the elastic properties of the model by means of the sound propagation. In the discrete model, the isotropy of the continuum equations and the proper values of the longitudinal and transverse wave speeds are recovered for perturbations with wavelengths typically above an order of magnitude larger than the lattice spacing.

The fracture criterion we have selected is extremely local (a single bond breaks at a time) and this, as far as comparisons with continuum theory are concerned, might be too simplistic. The idea is that local criteria, in which a single bond breaks at a time, must necessarily be subject to the local topology of the lattice. If the lattice is sought as a discretization of the continuum, one would expect that the lattice spacing should be much smaller than any other relevant length scale in the system (at least by a factor of 10). If the simplistic view of ''grains'' that break apart is taken, it is apparent that in an event of separation of grains, many lattice points would break at a time. In any case, it seems interesting to study new models with nonlocal criteria of fracture in which the decision to break a bond is taken from the dynamical state of many neighboring particles and not only from the couple that forms the bond.

Regarding the phenomenology of crack propagation, we have observed that fractures propagating in this model do not necessarily follow the lattice directions. There are, however, some effects of the lattice in the propagation of the cracks. Sometimes a dynamical trapping forces the crack to follow prescribed lattice directions. The origin of this lattice trapping effect might be attributed to the local criteria of fracture that we have selected.

We have seen that all cracks in this model of brittle linear elasticity accelerate and display branching when the crack tip speed exceeds a critical velocity of $c^*=0.7V_R$ for the Poisson ratio here considered. This critical value does not depend on the notch length and is close to the one obtained from Yoffe's hoop stress [18,1]. After the cracks branch, large fluctuations of the crack speed appear. These fluctuations are

very similar to the ones observed in experiments where the tip velocity is monitored by means of the resistance of a conductive thin film deposited on one of the faces of the test plate. According to our simulations, these fluctuations might be interpreted as an artifact of the measurement method that does not distinguish between simultaneously running branches of the same crack.

Even though a direct comparison between the theoretical stress field and the simulation results is difficult due to strong lattice effects, we have shown that these effects are to a large extent systematic. Its basic origin is due to anisotropy induced by the particular orientation of the breaking bond. In this way, we observe in the simulations that the stress field near the tip of the crack ''alternates'' between two almost mirror symmetric configurations as the crack snaps bonds of different orientations as it proceeds. It is remarkable that when this effect is removed from the representation of the stress fields by taking appropriate ratios at different times, the similarity with the theoretical results is much increased. It is tempting to speculate that this alternating configuration of the breaking bonds might introduce a component of Mode II loading close to the tip. Work to analyze this possibility in connection with the branching explanation given in [27] is in progress.

Even though from a qualitative point of view crack branching due to the Yoffe instability is an explanation for the observed low crack speed, it still does not explain *quantitatively* the experimental results. In fact, experiments show that there exist a critical crack speed above which the crack evolution is unstable (it oscillates, emits sound, and it microbranches). The typical value for this critical crack speed is significantly lower than that predicted by the Yoffe instability. Therefore, it is still an open question as to what are the essential ingredients that a model of brittle fracture should have in order to reproduce the experimental results.

Summarizing, we have investigated in this paper a simple model of linear elasticity with a local threshold criterion of fracture. It might be necessary to resort to more complex constitutive equations that can equally be treated with the general discretization method proposed in this paper. It seems also necessary to consider new criteria of fracture, which model in a more realistic way the complex physic that occur in the crack tip. From a computational point of view, nonlocal criteria are needed if the effects of the lattice are required to be negligible.

ACKNOWLEDGMENTS

We appreciate useful discussions and exchange of reports with F. Guinea, O. Pla, E. Louis, and L. Sander. This work has been partially supported by DGYCIT Project No. PB97-0077 and DGYCIT Project No. PB96-0148.

APPENDIX: DISCRETIZATION OF CONTINUUM EQUATIONS

In this Appendix we formulate the problem of discretizing the equations of elasticity on an arbitrary mesh as a problem of optimization. The method presented in this Appendix is, however, not restricted to the elasticity equations and can be applied to any set of partial differential equations.

Let $f(\mathbf{r})$ be any scalar field in $\mathbf{R}^D$ and consider a sample of M points distributed arbitrarily in the vicinity of a given point $\mathbf{r}_0$ with positions $\mathbf{r}_j$. The value of the scalar field at those points is denoted by $f_j = f(\mathbf{r}_j)$. The question we answer in this Appendix is, from our knowledge of $\mathbf{r}_i$ and f_i, which is the best estimate for the first and second derivatives of f at the point $\mathbf{r}_0$? This is a problem of optimization and essentially the solution consists of finding the best paraboloid that fits the points and contains the point $\mathbf{r}_0$, f_0 in $\mathbf{R}^{D+1}$. The equation of this paraboloid is

$$P(\mathbf{r}) = f_0 + \mathbf{A}\cdot(\mathbf{r}-\mathbf{r}_0) + \frac{1}{2}\mathbf{B}:(\mathbf{r}-\mathbf{r}_0)(\mathbf{r}-\mathbf{r}_0). \tag{A1}$$

A Taylor expansion of $f(\mathbf{r})$ around $\mathbf{r}_0$ shows that $\mathbf{A}$ is an approximation for the gradient of f at $\mathbf{r}_0$ and $\mathbf{B}$ is an approximation for the matrix of second derivatives. We construct then the optimization function

$$\begin{aligned}\phi(\mathbf{A},\mathbf{B}) &\equiv \sum_j^M [P(\mathbf{r}_j) - f_j]^2 \\ &= \sum_j^M \Big(f_0 - f_j + \mathbf{A}\cdot(\mathbf{r}_j-\mathbf{r}_0) \\ &\quad + \frac{1}{2}\mathbf{B}:(\mathbf{r}_j-\mathbf{r}_0)(\mathbf{r}_j-\mathbf{r}_0)\Big)^2. \end{aligned}\tag{A2}$$

By minimizing ϕ with respect to $\mathbf{A},\mathbf{B}$ we will obtain the paraboloid that best fits the points $\mathbf{r}_i, f_i$,

$$\begin{aligned} 0 &= \frac{\partial\phi}{\partial\mathbf{A}} = 2\left[-\mathbf{F}_1 + \mathbf{r}_2\cdot\mathbf{A} + \frac{1}{2}\mathbf{r}_3:\mathbf{B}\right], \\ 0 &= \frac{\partial\phi}{\partial\mathbf{B}} = \left[-\mathbf{F}_2 + \mathbf{r}_3\cdot\mathbf{A} + \frac{1}{2}\mathbf{r}_4:\mathbf{B}\right], \end{aligned}\tag{A3}$$

where we have defined

$$\begin{aligned} \mathbf{F}_1 &\equiv \sum_j^M (f_j - f_0)(\mathbf{r}_j-\mathbf{r}_0), \\ \mathbf{F}_2 &\equiv \sum_j^M (f_j - f_0)(\mathbf{r}_j-\mathbf{r}_0),(\mathbf{r}_j-\mathbf{r}_0), \end{aligned}\tag{A4}$$

which contain information about the function in the neighborhood of $\mathbf{r}_0$ and

$$\begin{aligned} \mathbf{R}_2 &\equiv \sum_j^M (\mathbf{r}_j-\mathbf{r}_0)(\mathbf{r}_j-\mathbf{r}_0), \\ \mathbf{R}_3 &\equiv \sum_j^M (\mathbf{r}_j-\mathbf{r}_0)(\mathbf{r}_j-\mathbf{r}_0)(\mathbf{r}_j-\mathbf{r}_0), \\ \mathbf{R}_4 &\equiv \sum_j^M (\mathbf{r}_j-\mathbf{r}_0)(\mathbf{r}_j-\mathbf{r}_0)(\mathbf{r}_j-\mathbf{r}_0), \end{aligned}\tag{A5}$$

which contain the topological information. The subindices on the **F**'s and **R**'s in (A4), (A5) denote the order of the tensorial quantity. The condition of minimum provides

$$\mathbf{R}_2\cdot\mathbf{A}+\frac{1}{2}\mathbf{R}_3:\mathbf{B}=\mathbf{F}_1,$$

$$\mathbf{R}_3\cdot\mathbf{A}+\frac{1}{2}\mathbf{R}_4:\mathbf{B}=\mathbf{F}_2. \tag{A6}$$

This is a system of linear equations for the $D+D(D+1)/2$ unknowns $\mathbf{A},\mathbf{B}$ (note that $\mathbf{B}$ is symmetric).

If, instead of first *and* second derivatives, only first derivatives were required, we would have started the problem by fitting the best *plane* (instead of paraboloid). This corresponds to the above formulas with $\mathbf{B}=0$. One could think that, then, second derivatives could be obtained by successive application of the formulas for the first derivatives. However, this has the drawback of bringing the neighbors of the neighbors of a given point into the expressions. This in general produces less accurate expressions for the derivatives. One can get a glimpse of this point by considering the one-dimensional (1D) case with equidistant points: The successive application of the first derivative expression produce the following approximation for the second derivative term $f_i''\approx(f_{i+2}+f_{i-2}-2f_i)/4a^2$, whereas the paraboloid expression produces the better approximation $f_i''\approx(f_{i+1}+f_{i-1}-2f_i)/2a^2$. For the same reason, if in a physical problem higher spatial derivatives appear, the procedure will consist of fitting higher order polynomials in order to obtain closed expressions for these higher order derivatives in terms of the values of the function in the neighbor points.

We will consider in this paper only near neighbors in a regular triangular lattice of spacing a in order to construct the discrete derivatives. We introduce the lattice vectors

$$\mathbf{r}_1=a(0,1)=-\mathbf{r}_4,$$

$$\mathbf{r}_2=a\left(\sqrt{\frac{3}{2}},\frac{1}{2}\right)=-\mathbf{r}_5,$$

$$\mathbf{r}_3=a\left(\sqrt{\frac{3}{2}},-\frac{1}{2}\right)=-\mathbf{r}_6 \tag{A7}$$

in such a way that

$$\mathbf{R}_2=\sum_{i=1}^{6}\mathbf{r}_i\mathbf{r}_i=2\sum_{i=1}^{3}\mathbf{r}_i,\mathbf{r}_i=3a^2\mathbf{1},$$

$$\mathbf{R}_3=\sum_{i=1}^{6}\mathbf{r}_i\mathbf{r}_i\mathbf{r}_i=\sum_{i=1}^{3}\mathbf{r}_i\mathbf{r}_i\mathbf{r}_i+\sum_{i=4}^{6}\mathbf{r}_i\mathbf{r}_i\mathbf{r}_i=0,$$

$$\mathbf{R}_4=\sum_{i=1}^{6}\mathbf{r}_i\mathbf{r}_i\mathbf{r}_i\mathbf{r}_i=2\sum_{i=1}^{3}\mathbf{r}_i\mathbf{r}_i\mathbf{r}_i\mathbf{r}_i. \tag{A8}$$

The last fourth order tensor is symmetric in all its indices and then we only need to consider $R^{1111},R^{1112},R^{1122},R^{1222},R^{2222}$. The final result is

$$\mathbf{R}^{\mu\nu\sigma\gamma}=\frac{3}{4}a^4[\,\delta^{\mu\nu}\delta^{\sigma\gamma}+\delta^{\mu\sigma}\delta^{\nu\gamma}+\delta^{\mu\gamma}\delta^{\nu\sigma}]. \tag{A9}$$

Inserting (A8), (A9) into (A6) we arrive at

$$3a^2\mathbf{A}=\mathbf{F}_1,$$

$$\frac{3}{8}a^4[\mathbf{1}\,\mathrm{tr}\,\mathbf{B}+2\mathbf{B}]=\mathbf{F}_2, \tag{A10}$$

By taking the trace of the last equation we have

$$\mathrm{tr}\,\mathbf{B}=\frac{2}{3a^4}\,\mathrm{tr}\,\mathbf{F}_2, \tag{A11}$$

and substituting back into (A10)

$$\mathbf{A}=\frac{1}{3a^2}\mathbf{F}_1,$$

$$\mathbf{B}=\frac{4}{3a^4}\left[\mathbf{F}_2-\frac{1}{4}(\mathrm{tr}\,\mathbf{F}_2)\mathbf{1}\right]. \tag{A12}$$

This is

$$\mathbf{A}=\frac{1}{3}\sum_{j=1}^{6}\frac{f_j-f_0}{a}\hat{\mathbf{r}}_j^0,$$

$$\mathbf{B}=\frac{4}{3}\sum_{j=1}^{6}\frac{f_j-f_0}{a^2}\hat{\mathbf{r}}_j^0\hat{\mathbf{r}}_j^0-\frac{1}{3}\sum_{j=1}^{6}\frac{f_j-f_0}{a^2}\mathbf{1}, \tag{A13}$$

where $\hat{\mathbf{r}}_j^0=(\mathbf{r}_j-\mathbf{r}_0)/a$. The Laplacian is given by the trace of $\mathbf{B}$, which from (A11) is

$$\mathrm{tr}\,\mathbf{B}=\frac{2}{3}\sum_{j=1}^{6}\frac{f_j-f_0}{a^2}. \tag{A14}$$

The advantage of the formalism presented is that the derivatives appear in a tensorial formulation from the outset. The gradient of a function is a vector involving the value of the function and the relative position vectors of the neighbor points, whereas the matrix of second derivatives is a second order tensor. One can write the expression in component form in order to make contact with usual formulations of finite differences algorithms. For example, in a triangular lattice with lattice vectors given by (A7) the gradient is given by

$$\mathbf{A}_i^x=(\partial_x f)_i=\frac{1}{6}\left(4\frac{f_1-f_4}{2a}+\frac{f_2-f_3}{2a}+\frac{f_6-f_5}{2a}\right),$$

$$\mathbf{A}_i^y=(\partial_y f)_i=\frac{1}{2}\left(\frac{f_2-f_6}{\sqrt{3}a}+\frac{f_3-f_5}{\sqrt{3}a}\right), \tag{A15}$$

which is a weighted average between the different possible differences in the appropriate directions.

Finally, in a triangular lattice, the equations (1) have the following spatial discretization in a particular node i,

$$\ddot{\mathbf{u}}_i(t)=\left[\frac{c_\perp^2-c_\parallel^2/3}{a^2}\right]\sum_{j=1}^{6}(\mathbf{u}_j-\mathbf{u}_i)+\frac{4(c_\parallel^2-c_\perp^2)}{3a^2}\sum_{j=1}^{6}(\mathbf{u}_j-\mathbf{u}_i)\cdot\hat{\mathbf{r}}_{ji}^0\hat{\mathbf{r}}_{ji}^0. \tag{A16}$$

[1] L. B. Freund, *Dynamic Fracture Mechanics* (Cambridge University Press, New York, 1990).

[2] *Random fluctuations and Pattern Growth: Experiments and Models*, edited by H. E. Stanley and N. Ostrowsky (Kluwer Academic, Dordrecht, 1988); *Statistical Models for the Fracture of Disordered Media*, edited by H. J. Herrmann and S. Roux (North Holland, Amsterdam 1990).

[3] J. Fineberg, S. P. Gross, M. Marder, and H. L. Swinney, Phys. Rev. Lett. **67**, 457 (1991).

[4] S. P. Gross, J. Fineberg, M. Marder, W. D. McCormick, and H. L. Swinney, Phys. Rev. Lett. **71**, 3162 (1993).

[5] E. Sharon, S. P. Gross, and J. Fineberg, Phys. Rev. Lett. **74**, 5096 (1995).

[6] J. F. Boudet, V. Steinberg, and S. Ciliberto, Europhys. Lett. **30**, 337 (1995); J. F. Boudet, S. Ciliberto, and V. Steinberg, J. Phys. II **6**, 1493 (1996).

[7] J. F. Boudet and S. Ciliberto, Phys. Rev. Lett. **80**, 341 (1998).

[8] J. S. Langer, Phys. Rev. Lett. **70**, 3592 (1993); J. S. Langer and H. Nakanishi, Phys. Rev. E **48**, 439 (1993).

[9] H. Gao, J. Mech. Phys. Solids **41**, 457 (1993).

[10] Sh. A. Kulkhmetova, V. A. Saraikin, and L. I. Slepyan, Mech. Solids **19**, 101 (1984); M. Marder and X. Liu, Phys. Rev. Lett. **71**, 2417 (1993); M. Marder and S. P. Gross, J. Mech. Phys. Solids **43**, 1 (1995).

[11] W. T. Ashurst and W. G. Hoover, Phys. Rev. B **14**, 1465 (1976).

[12] F. F. Abraham, D. Brodbeck, R. A. Rafey, and W. E. Rudge, Phys. Rev. Lett. **73**, 272 (1994); B. L. Hoolian and R. Ravelo, Phys. Rev. B **51**, 11 275 (1995); S. J. Zhou, P. S. Lomdahl, R. Thomson, and B. L. Holian, Phys. Rev. Lett. **76**, 2318 (1996); F. F. Abraham, *ibid.* **77**, 869 (1996); A. Omeltchenko, J. Yu, R. K. Kalia, and P. Vashishta, *ibid.* **78**, 2148 (1997); D. Holland and M. Marder, *ibid.* **80**, 746 (1998).

[13] O. Pla, F. Guinea, E. Louis, S. V. Ghaisas, and L. M. Sander, Phys. Rev. B **57**, 981 (1998).

[14] X.-P. Xu and A. Needleman, J. Mech. Phys. Solids **42**, 1397 (1994).

[15] M. Born and K. Huang, *Dynamical Theory of Crystal Lattices* (Oxford University Press, London, 1954).

[16] H. Yan, G. Li, and L. M. Sander, Europhys. Lett. **10**, 7 (1989); G. Caldarelli, C. Castellano, and A. Vespignani, Phys. Rev. E **49**, 2673 (1994).

[17] M. P. Allen and D. J. Tildesley, *Computer Simulation of Liquids* (Clarendon Press, Oxford, 1987).

[18] E. H. Yoffe, Philos. Mag. **42**, 739 (1951).

[19] M. Adda-Bedia, M. Ben Amar, and Y. Pomeau, Phys. Rev. E **54**, 5774 (1996).

[20] L. D. Landau and E. M. Lifshitz, *Theory of Elasticity* (Pergamon Press, New York, 1986).

[21] M. L. Williams, J. Appl. Mech. **24**, 109 (1957); B. R. Baker, *ibid.* **29**, 449 (1962).

[22] Results on simulations with discretizations including next nearest neighbors will be reported separately.

[23] F. Tzschichholz, Phys. Rev. B **52**, 9270 (1995).

[24] P. Español, M. A. Rubio, and I. Zúñiga, Physica D **96**, 375 (1996). A preliminary account was given in P. Español, M. A. Rubio, and I. Zúñiga, Mater. Res. Soc. Symp. Proc. **409**, 101 (1995).

[25] W. G. Knauss, J. Appl. Mech. 356 (1966).

[26] H. A. Posch, W. G. Hoover, and O. Kum, Phys. Rev. E **52**, 1711 (1995).

[27] M. Adda-Bedia, R. Arias, M. Ben Amar, and F. Lund, Phys. Rev. Lett. **82**, 2318 (1999).